



**FACULTY
OF MATHEMATICS
AND PHYSICS**
Charles University

BACHELOR THESIS

Martin Vavřík

**Simulation and Reconstruction
of Charged Particle Trajectories
in an Atypic Time Projection Chamber**

Institute of Particle and Nuclear Physics

Supervisor of the bachelor thesis: Mgr. Tomáš Sýkora, Ph.D.

Study programme: Physics

Prague 2025

9 I declare that I carried out this bachelor thesis independently, and only with the
10 cited sources, literature and other professional sources. It has not been used to
11 obtain another or the same degree.

12 I understand that my work relates to the rights and obligations under the Act
13 No. 121/2000 Sb., the Copyright Act, as amended, in particular the fact that the
14 Charles University has the right to conclude a license agreement on the use of this
15 work as a school work pursuant to Section 60 subsection 1 of the Copyright Act.

In date
Author's signature

Title: Simulation and Reconstruction of Charged Particle Trajectories in an Atypical Time Projection Chamber Added hyphen to avoid overfull hbox

Author: Martin Vavřík

Institute: Institute of Particle and Nuclear Physics

Supervisor: Mgr. Tomáš Sýkora, Ph.D., Institute of Particle and Nuclear Physics

Abstract: Abstract.

Keywords: key words

Contents

17		
18	Motivation	2
19	0.1 ATOMKI Measurements	2
20	0.2 X17 Project at IEAP CTU	2
21	1 Time Projection Chamber	3
22	1.1 Orthogonal Fields TPC at IEAP CTU	3
23	1.1.1 Coordinate Systems	3
24	1.1.2 Magnetic Field Simulation	4
25	2 Track Simulation	7
26	2.1 Microscopic Simulation	7
27	2.2 Runge-Kutta Simulation	8
28	3 Track Reconstruction	9
29	3.1 Reconstruction Assuming Steady Drift	9
30	3.2 Ionization Electron Map	11
31	3.2.1 Gradient Descent Search	14
32	3.2.2 Interpolation on the Inverse Grid	15
33	3.3 Discrete Reconstruction	16
34	4 Energy Reconstruction	18
35	4.1 Cubic Spline Fit	18
36	4.2 Circle and Lines Fit	20
37	4.2.1 Two-dimensional fit	20
38	4.2.2 Three-dimensional fit	22
39	4.3 Runge-Kutta Fit	22
40	Conclusion	24
41	Bibliography	26
42	List of Figures	27
43	List of Tables	28
44	List of Abbreviations	29

Motivation

A Time Projection Chamber (TPC) is a type of gaseous detector that detects charged particle trajectories by measuring the positions and drift time of ions created in the gas; details are provided in Section 1. The energy of these particles can be inferred from the curvature of their trajectory in the magnetic field.

The goal of this thesis is to develop an algorithm for the reconstruction of charged particle trajectories and energy in an atypic TPC with orthogonal electric and magnetic fields, hereafter referred to as the Orthogonal Fields TPC (OFTPC), used in the X17 project at the Institute of Experimental and Applied Physics, Czech Technical University in Prague (IEAP CTU). Furthermore, we present the results of testing this algorithm with different samples of simulated data. We use the Garfield++ toolkit [1] for simulations in combination with the ROOT framework [2] for data analysis and visualization. Some of our more demanding simulations are run on the MetaCentrum grid.

The X17 project in IEAP CTU aims to reproduce measurements of anomalous behavior in the angular correlation distribution of pairs produced by the Internal Pair Formation (IPF) mechanism during the decay of certain excited nuclei (^8Be , ^{12}C , and ^4He) observed by the ATOMKI group in Hungary. I would leave this here as a short summary before I explain it in more detail in the sections below.

Add citations: MetaCentrum, X17 project, VdG, ATOMKI papers. Maybe also TPC, IPF, etc.

0.1 ATOMKI Measurements

Short summary of results of measurements in ATOMKI.

0.2 X17 Project at IEAP CTU

Short summary of our goals, maybe mention the grant.

1. Time Projection Chamber

Description of TPC, working principle, standard vs. our field layout.

1.1 Orthogonal Fields TPC at IEAP CTU

Short description of our detector. Why we use an atypic TPC (benefits, complications). Gas mixture used in the detector (70/30) and its effect.

1.1.1 Coordinate Systems

In order to describe events in our detector, we use three distinct spaces: the detector space \mathcal{D} , the readout space \mathcal{R} and the pad space \mathcal{P} . Each space is later used to represent ionization electrons at different stages of the detection process: their creation in the gas, their final position when hitting the readout plane, and finally their representation in the discrete pad space.

Detector Space

The detector space \mathcal{D} represents the physical space of our detector. We describe it using Cartesian coordinates (x, y, z) . The z -axis is the detector's axis of symmetry, with its negative direction aligned with the proton beam. The origin $(0, 0, 0)$ is located at the center of the irradiated target. The positive x -axis passes through the center of one of the OFTPCs along the intersection of its two planes of symmetry. The y -axis is then chosen to maintain a right-handed coordinate system.

Since the detector has a hexagonal symmetry, we use only one of its sectors in this work – the first sector $\mathcal{D}_1 \subset \mathcal{D}$ which is defined by the condition:

$$(x, y, z) \in \mathcal{D}_1 \Leftrightarrow |y| \leq x \tan \frac{\pi}{6}. \quad (1.1)$$

Simulations in this sector can be applied to all sectors by rotating the coordinates accordingly. The volume of the OFTPC in this sector, which has the shape of a trapezoidal prism, has these boundaries:

$$x \in [x_{\min}, x_{\max}] = [6.51, 14.61] \text{ cm}, \quad (1.2)$$

$$z \in [z_{\min}, z_{\max}] = [-8, 8] \text{ cm}, \quad (1.3)$$

$$y_{\max}(x_{\min}) = -y_{\min}(x_{\min}) = 2.75 \text{ cm}, \quad (1.4)$$

$$y_{\max}(x_{\max}) = -y_{\min}(x_{\max}) = 7.45 \text{ cm}, \quad (1.5)$$

where $y_{\max}(x)$ is the maximal value of the y -coordinate for a given x . The readout is located at $z = 8 \text{ cm}$; for some purposes, we also define the distance to the readout $d_r = 8 \text{ cm} - z$ as an alternative to the z -coordinate. **Keeping this paragraph as it is because the OFTPC volume is distinct from the first sector and some parts of this thesis use the space beyond this volume.**

100 Readout Space

101 The readout space \mathcal{R} represents the drift time and final positions of ionization
 102 electrons as measured by an ideal continuous readout. We describe it using
 103 coordinates (x', y', t) , where x' and y' correspond to the detector coordinates at
 104 the readout plane ($z = 8$ cm). **Currently not entirely sure how to put this into**
 105 **a figure since only x' and y' correspond to the detector coordinates. The drift**
 106 **time t is approximately proportional to d_r .**

107 Pad Space

108 The pad space \mathcal{P} represents the time bin and pad number of ionization electrons
 109 as measured by an ideal discrete readout. **It is not really a subspace of \mathcal{R} but**
 110 **there is a mapping from \mathcal{R} to \mathcal{P} . It is a discretization of a part of \mathcal{R} , the mapping**
 111 **can be adjusted depending on the simulation. If we assume uniform electric field**
 112 **there will be gaps, we don't use gaps in the reconstruction since the electrons**
 113 **should be pulled towards the pads.**

114 The readout of the OFTPC will consist (**is the design final?**) of 128 rectangular
 115 pads arranged in a staggered pattern (**add image where all the parameters are**
 116 **marked**). Most of the pads are 0.6×0.9 cm, only pads 102 and 124 are 0.6×0.6 cm,
 117 pad 127 is 0.6×0.509 cm. The distance of neighboring pads is 0.08 cm, staggering
 118 offset is 0.3946 cm.

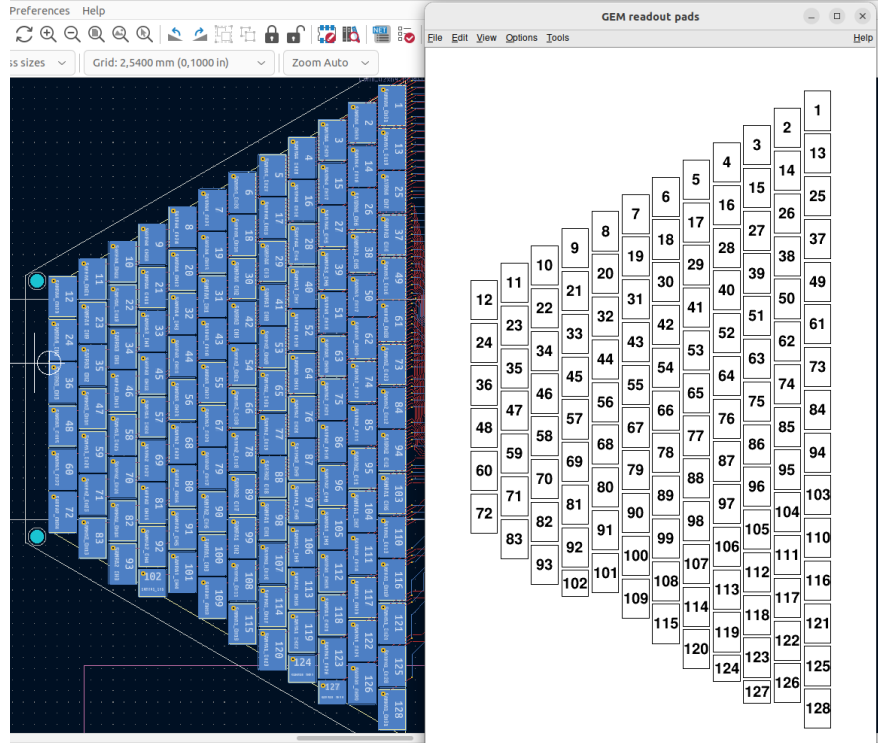


Figure 1.1: Pad layout of the TPC. **Swap for better image.**

119 1.1.2 Magnetic Field Simulation

120 **Magnetic field simulations in Maxwell (citation). Some figures. When working**
 121 **with the magnetic field outside the regular grid, we use trilinear interpolation.**

122 Trilinear Interpolation

123 Trilinear interpolation is a 3D generalization of linear interpolation. It can be
 124 used to interpolate a function whose values are known on a regular grid with
 125 rectangular prism cells. We use this simple method for interpolating the magnetic
 126 field, and it is later used in Section 3.2.1 to interpolate the Ionization Electron
 127 Map, a key component of our track reconstruction algorithm. In both cases, we
 128 use a regular cubic grid (apparently it is also called a Cartesian grid).

129 Could put a paragraph about linear interpolation here if it is not clear from
 130 the equations below.

131 Let us consider a cell of our regular grid (a cube) with an edge of length a
 132 containing the point $\mathbf{C} = (x, y, z)$ where we want to interpolate a function
 133 $f: \mathbb{R}^3 \rightarrow \mathbb{R}$. We know the values of this function at the vertices of the cell
 134 $\mathbf{C}_{ijk} = (x_0 + ia, y_0 + ja, z_0 + ka)$, where $i, j, k \in \{0, 1\}$ are indices. We also define
 135 the points $\mathbf{C}_{ij} = (x, y_0 + ia, z_0 + ja)$ and $\mathbf{C}_i = (x, y, z_0 + ia)$. Then the interpolated
 136 value $\hat{f}(\mathbf{C})$ can be calculated as a composition of three linear interpolations (see
 137 Figure 1.2):

$$\hat{f}(\mathbf{C}_{ij}) = (1 - x_d) f(\mathbf{C}_{0ij}) + x_d f(\mathbf{C}_{1ij}), \quad (1.6)$$

$$\hat{f}(\mathbf{C}_i) = (1 - y_d) \hat{f}(\mathbf{C}_{0i}) + y_d \hat{f}(\mathbf{C}_{1i}), \quad (1.7)$$

$$\hat{f}(\mathbf{C}) = (1 - z_d) \hat{f}(\mathbf{C}_0) + z_d \hat{f}(\mathbf{C}_1), \quad (1.8)$$

138 where x_d, y_d , and z_d are given as follows:

$$x_d = \frac{x - x_0}{a}, \quad y_d = \frac{y - y_0}{a}, \quad z_d = \frac{z - z_0}{a}. \quad (1.9)$$

139 We can also write

$$\hat{f}(\mathbf{C}) = \sum_{i,j,k \in \{0,1\}} t_x^i t_y^j t_z^k f(\mathbf{C}_{ijk}), \quad (1.10)$$

$$t_\alpha \stackrel{\text{def}}{=} \begin{pmatrix} t_\alpha^0 \\ t_\alpha^1 \end{pmatrix} = \begin{pmatrix} 1 - \alpha_d \\ \alpha_d \end{pmatrix}, \quad (1.11)$$

140 where $\alpha \in \{x, y, z\}$ is an index. Furthermore, we can write $\hat{f}(\mathbf{C})$ as a polynomial:

$$\hat{f}(\mathbf{C}) = \sum_{\alpha, \beta, \gamma \in \{0,1\}} \sum_{i=0}^{\alpha} \sum_{j=0}^{\beta} \sum_{k=0}^{\gamma} (-1)^{(\alpha-i)+(\beta-j)+(\gamma-k)} f(\mathbf{C}_{ijk}) x_d^\alpha y_d^\beta z_d^\gamma. \quad (1.12)$$

141 We take advantage of this form when generalizing trilinear interpolation to irreg-
 142 ular grid in section 3.2.2.

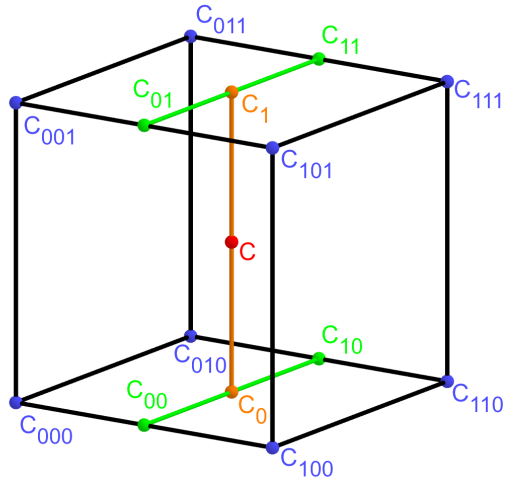


Figure 1.2: Visualization of trilinear interpolation as a composition of linear interpolations. Image drawn in GeoGebra and inspired by a similar image on Wikipedia (which looks a bit worse) – is credit necessary?

143 Maybe a citation here, although I am not sure it is necessary since it could
 144 be considered common knowledge. The last two equations are my own. Maybe
 145 x_0 , etc. should be explicitly described.

2. Track Simulation

In order to develop and test the reconstruction algorithm, electron and positron tracks are simulated inside the first sector \mathcal{D}_1 of our detector (see Section 1.1.1) with different initial parameters. Two approaches are currently used to simulate tracks, each of them for different purpose.

The **Microscopic Simulation** uses the Garfield++ toolkit [1]. Within this toolkit, the High Energy Electro-Dynamics (HEED) program [3] is used to simulate the primary particle and the class *AvalancheMicroscopic* to simulate the drift of secondary electrons created by ionization in the gas. This is the most precise and time-consuming simulation used; our current goal is to be able to successfully reconstruct its results and determine our best-case energy resolution.

The **Runge-Kutta Simulation** uses the 4th order Runge-Kutta numerical integration (add citation for Runge-Kutta) to simulate the trajectory of the primary particle in the electromagnetic field inside the detector. It is relatively fast since it does not simulate the secondary particles. It is used as part of our reconstruction algorithm and for testing some parts of the reconstruction.

All of these simulations require the knowledge of the electromagnetic field inside the detector. A uniform electric field of $400 \text{ V}\cdot\text{cm}^{-1}$ is assumed. The magnetic field was simulated in Maxwell (see Section 1.1.2). add citation

Single track in positive x direction or initial parameter randomization. Importance of gas composition, used gas compositions.

2.1 Microscopic Simulation

The microscopic simulation, the most detailed simulation used in this work, is performed using the Garfield++ toolkit [1].

The electron transport properties are simulated using the program Magboltz (Add citation.). Two different gas mixtures were used: 90% Ar + 10% CO₂ and 70% Ar + 30% CO₂. The second mixture will be used in our detector. The temperature is set to 20 °C, the pressure is atmospheric.

The primary track is simulated using the program HEED [3], which is an implementation of the photo-absorption ionization model. This program provides the parameters of ionizing collisions. HEED can also be used to simulate the transport of delta electrons; we do not account for these in the current simulation but plan to include them in the future. The photons created in the atomic relaxation cascade (fluorescence reabsorption, ?) are also not simulated.

Finally, we use the microscopic tracking provided by the class *AvalancheMicroscopic* to simulate the drift of the ionization electrons. Each electron is followed from collision to collision using the equation of motion and the collision rates calculated by Magboltz.

First simulated track in the z direction should be described in detail here (own subsection?). Figures.

Add more detailed and better description of HEED, and microscopic tracking (each their own subsection?). Could also mention Monte Carlo (requires gas file generation) and Runge-Kutta simulation implemented in Garfield, why we don't

189 use them (another subsection? rename the section to Garfield++ simulation and
 190 mention all relevant parts?).

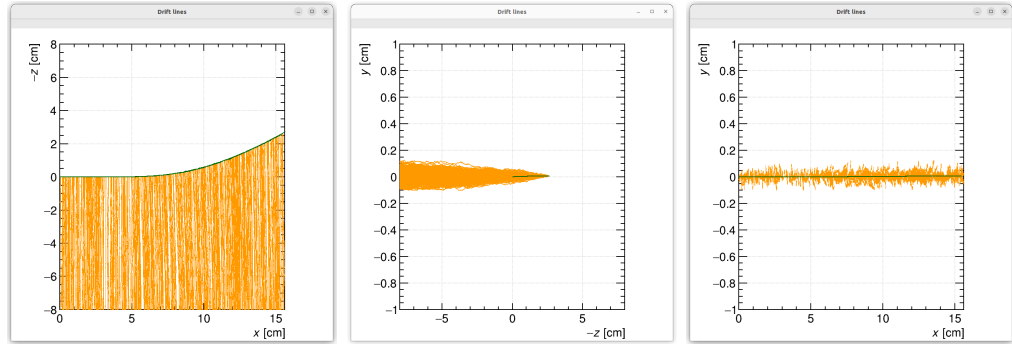


Figure 2.1: Example of a simulated electron track in 70 % argon and 30 % CO₂ atmosphere (on the left). Swap for better images, better zoom. Explain drift lines, primary particle.

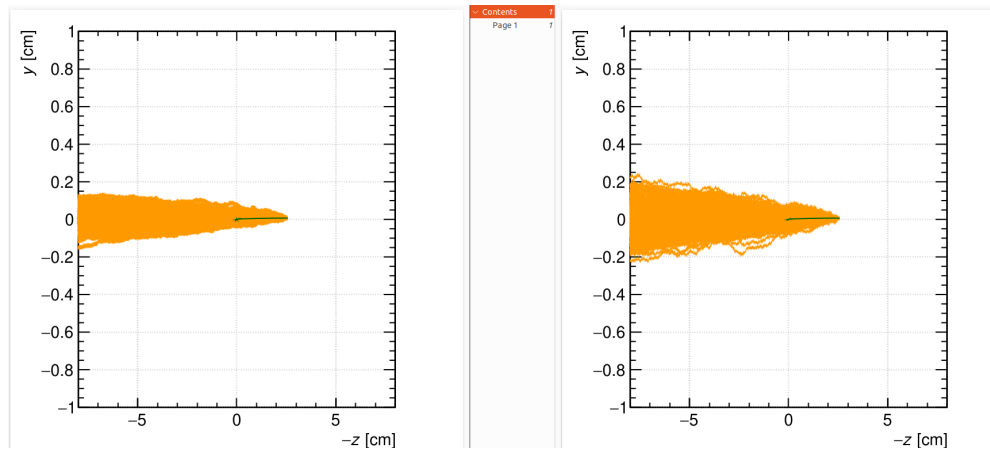


Figure 2.2: Comparison of diffusion in a simulated electron track in 70 % argon, 30 % CO₂ atmosphere and in 90 % argon, 10 % CO₂ atmosphere (on the right). Swap for better image, better zoom. Or put the same pictures for both comparisons in one subfigure, etc. Describe better.

191 2.2 Runge-Kutta Simulation

192 Trajectory simulation with 4th order Runge-Kutta. Relativistic equation that is
 193 numerically integrated by the algorithm.

194 3. Track Reconstruction

195 In the first stage of the reconstruction algorithm, we reconstruct the track of
 196 a primary particle (either an electron or a positron). The result of this step is
 197 then used to determine the energy of the particle (Section 4).

198 The **Reconstruction Assuming Steady Drift** uses the standard TPC ap-
 199 proach. With parallel fields, the drift inside a uniform electric field remains
 200 undistorted (reference to some future part of the TPC chapter). Therefore, we
 201 only need to reconstruct the z -coordinate from the drift time using the known
 202 drift velocity. We also assume that the readout coordinates (x', y', t) are known
 203 exactly, neglecting the pads and time bins.

204 Reconstruction using the **Ionization Electron Map** (from now on referred
 205 to as *the map*) uses a simulation of the drift of secondary (ionization) electrons
 206 within the detector volume. This simulation can then be used to interpolate
 207 the initial position of the secondary electrons. First attempts neglect the pads.

208 We use the map for reconstruction in two different ways. The first one uses
 209 gradient descent search along with trilinear interpolation (see Section 1.1.2) of
 210 the map. The second method uses interpolation on the irregular inverse grid with
 211 a linear polynomial.

212 The **Discrete Reconstruction** uses the map; instead of reconstructing the ex-
 213 act position of each electron, we reconstruct the center of each hit pad with
 214 the time corresponding to the midpoint of the time bin. The electron count in
 215 each TPC bin (consisting of the pad and the time bin) serves as the charge value,
 216 which is then used as a weight in the energy reconstruction fit.

217 3.1 Reconstruction Assuming Steady Drift

218 As the first step, we decided to try to reconstruct an electron track with a special
 219 set of initial parameters. The origin of the particle is given by the origin of our
 220 coordinate system. The initial direction is given by the positive x -axis. This
 221 means the magnetic field of our detector is perpendicular to the momentum of
 222 the particle at all times, and we can reduce the problem to two-dimensional space.
 223 As an example, we use a track simulated using the microscopic simulation (see
 224 Section 2.1) with a kinetic energy of 8 MeV. The gas composition used in this
 225 simulation is 90% Ar + 10% CO₂. Might be better to describe this track in
 226 Section 2.1.

227 In this approach to the reconstruction of the track, we decided to use the com-
 228 mon method used in a standard TPC. This will allow us to explore the significance
 229 of the atypical behavior in our OFTPC. Additionally, we assume the readout is
 230 continuous to further simplify the problem. In this approximation, we reconstruct
 231 the initial position of each ionization electron.

232 The reconstruction is then defined by the following relations between the co-
 233 ordinates of the detector space and the readout space (see Section 1.1.1):

$$x = x', \quad (3.1)$$

$$y = y', \quad (3.2)$$

$$z = v_d t, \quad (3.3)$$

234 where v_d is the drift velocity of electrons in the given gas mixture. At a phe-
 235 nomenological level, this velocity can be considered as a function of the electric
 236 field \mathbf{E} and the magnetic field \mathbf{B} :

$$v_d = v_d(\mathbf{E}, \mathbf{B}). \quad (3.4)$$

237 Equation taken from Garfield user manual. The Garfield++ toolkit uses this
 238 fact to accelerate their drift simulation with non-microscopic approaches (could
 239 mention in the simulation chapter). Since we assume a uniform electric field in
 240 our detector and we want to neglect the effect of our unusual magnetic field, we
 241 consider the drift velocity to be constant in this scenario. We then approximate
 242 this velocity by fitting the dependence $z(t)$ taken from the simulated ionization
 243 electrons. This is in one of the provisional figures. Also, this description is
 244 not completely accurate; in reality, we fit $t1:8-y0$ with $a1*x+a0$ and then invert
 245 this and use $8-y0 = b1*t1+b0$ (old coordinates); $b1=1/a1$ functions as the drift
 246 velocity. Maybe also define this 8-z variable as an alternative to z in Section 1.1.1
 247 and then use it when correcting this.

248 Later, in a commit after this, I plotted some residues (provisional figure),
 249 which could be useful, but for some reason they are residuals from a spline fit of
 250 the track?! Probably redo this without the spline fit; just explore the difference
 251 in individual points.

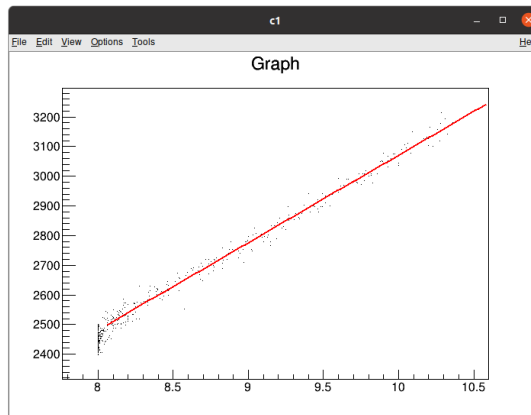


Figure 3.1: Dependence of the drift time on the z coordinate in 90 % argon and 10 % CO_2 atmosphere, fitted with a linear function. The fitted function gives us the average drift velocity in the gas and can be used for rough reconstruction in our TPC. Swap for better image with axis labels, etc. Maybe write the fitted equation.

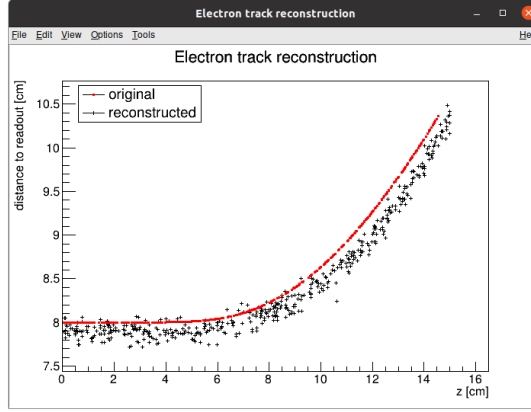


Figure 3.2: First attempt at a track reconstruction using only the drift velocity. This approach works well in a standard TPC (ideally cite some source?). 90 % argon and 10 % CO₂ atmosphere. Swap for better image, correct coordinates.

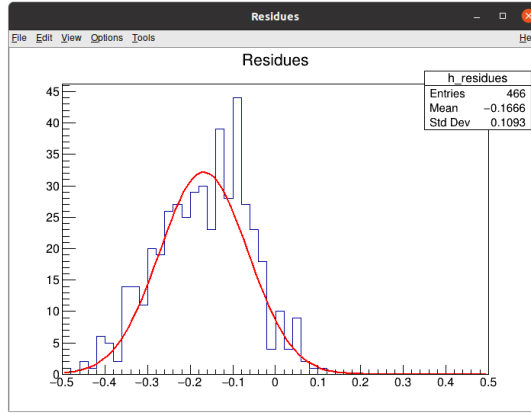


Figure 3.3: First attempt at a track reconstruction using only the drift velocity, residues. Swap for better image, correct coordinates. What's causing the shift? Explain details.

3.2 Ionization Electron Map

Inside an OFTPC, the drift of the secondary (ionization) electrons is significantly affected by its magnetic field (pictures of the distortion later, the effect is bigger for the 90/10 composition). We need to take this into account for accurate reconstruction. In the first approximation, we assume a continuous readout (i.e., we neglect pads). We can then reconstruct the original position of each ionization electron using its readout coordinates. For this purpose, we use the ionization electron map.

The ionization electron map represents a mapping from the detector space to the readout space (see Section 1.1.1). It tells us what readout coordinates (x', y', t) we can expect on average for an ionization electron created at the detector coordinates (x, y, z) . More precisely it is a mapping to the distributions on the readout space; we can simplify this as only the means \overline{M} and the covariance

265 matrices \mathcal{M}_{cov} , assuming Gaussian distribution.

$$\mathcal{M} : \mathcal{D} \longrightarrow \mathcal{R}, (x, y, z) \longmapsto (x', y', t). \quad (3.5)$$

266 To get an approximation of this mapping, we simulate the drift of ionization
 267 electrons generated on a regular grid inside the volume of our OFTPC ¹. It
 268 is also useful to simulate multiple (100 in our case) electrons originating from
 269 the same position so we can get a better information about the average drift
 270 and its variance. In order to get more accurate results, we use the microscopic
 271 simulation of these electrons described in Section 2.1. When evaluating the map
 272 inside the grid, we use trilinear interpolation (see Section 1.1.2). From now on,
 273 we will denote this interpolated simulation with the same symbol \mathcal{M} .

274 Finally, we need to invert the map to get the original detector coordinates
 275 (x, y, z) for the given readout coordinates (x', y', t) . In our case, we can reason-
 276 ably assume that the mapping $\overline{\mathcal{M}}$ is one-to-one (as seen in the simulations). We
 277 implemented two methods for this purpose: the gradient descent search (Sec-
 278 tion 3.2.1) and interpolation on the inverse grid (Section 3.2.2).

279 The simulation of the map is a computationally heavy task. For this reason, we
 280 use the MetaCentrum grid (citation) to parallelize needed calculations. At first,
 281 this was done by evenly distributing the simulated electrons across the individual
 282 jobs in a simulation with only one electron per vertex in the regular grid with
 283 a spacing of one centimeter.

284 Later, a more efficient approach was implemented, accounting for the varying
 285 lengths of the drift of individual electrons. If we index the electrons in the order
 286 of increasing coordinates y, x, z (picture?), we can express the number n_l of full
 287 XY layers (i.e., electrons with the same z coordinate) of electrons with index less
 288 than or equal to i

$$n_l(i) = \left\lfloor \frac{i}{n_{xy}} \right\rfloor, \quad (3.6)$$

289 where n_{xy} is the number of electrons in each XY layer calculated simply by count-
 290 ing the electrons that satisfy boundary conditions for x and y . These conditions
 291 should be mentioned above; sector condition + maximal x value. The number of
 292 electrons remaining in the top layer is then

$$n_r(i) = i \bmod n_{xy}. \quad (3.7)$$

293 Finally, we can calculate the sum of the drift gaps of electrons up to index i

$$d_{\text{sum}} = (z_{\text{max}} - z_{\text{min}})n_{xy}n_l - \frac{n_l(n_l - 1)}{2}n_{xy}l + n_r(z_{\text{max}} - z_{\text{min}} - n_l l). \quad (3.8)$$

294 We then use a binary search algorithm to find the maximum index i such that
 295 the value of this sum is less than the fraction $\frac{\text{job id}}{\text{max job id}}$ of the total sum. This way
 296 we obtain the minimal and the maximal index of electrons simulated in the given
 297 job. The spacing l should be probably defined above + picture of the simulating
 298 grid (1 layer). zmin zmax also

299 After the simulation of the map, we calculate the mean readout coordinates
 300 assuming Gaussian distribution (i.e., we use averages). We also calculate standard

¹we do not take the detector walls into account and simulate even outside of the OFTPC which lets us interpolate even close to the walls

301 deviations in a later commit, should be upgraded to the covariance matrix. We
 302 never actually plotted the distributions we get when simulating the same electron
 303 multiple times, so we do not know if our assumptions are accurate (could also
 304 run some statistical test to see how well the Gaussian distribution fits).

305 The obtained map is then stored in a custom class template *Field*, could
 306 expand on that. Maybe earlier, since the same template is used for the magnetic
 307 field.

308 Could insert a table here describing all 4 simulations of the map (gas composi-
 309 tion, spacing, etc.). Simulation inside of one sector (at first double angle). Extra
 310 space on the sensor. Edge cases not taken into account (TPC wall). Using qsub
 311 (not sure if important). Add plots of distortion of the coordinates. Could also do
 312 these plots in a different way (e.g., drawing all the endpoints of each ionization
 313 electron or some error ellipse plot).

314 Images to add (comparison of both simulations):

- 315 • 3D visualization of the map, simulation example
- 316 • z vs. t plot
- 317 • XY plane distortion for different z values; with arrows and error bars, for
 318 all z -layers with different colors
- 319 • XZ plane ($y = 0$) distortion in x (maybe not necessary?)
- 320 • XT plot ($y = 0$) showing (small) distortion in drift times

321 More images:

- 322 • Residuals of the continuous readout reconstruction.

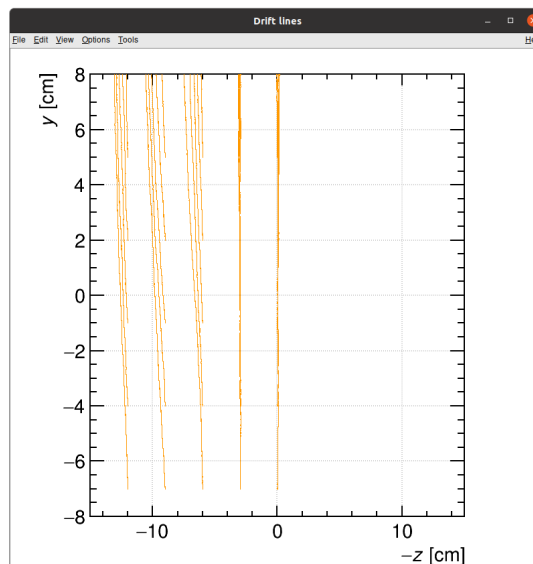


Figure 3.4: Example of map generation. Swap for better image, correct coordinates.

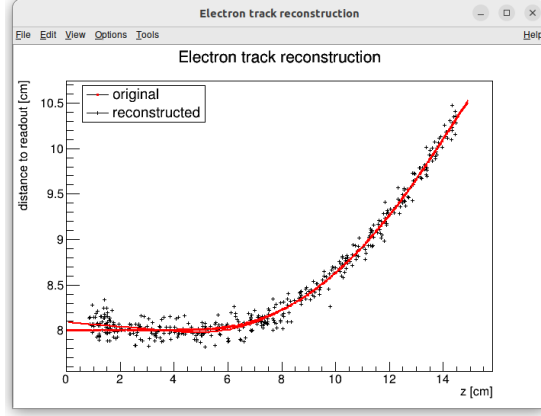


Figure 3.5: Example reconstruction with the map. **Swap for better image, correct coordinates.**

3.2.1 Gradient Descent Search

The first implemented method of reconstruction uses a gradient descent search to calculate an inversion of the map $\bar{\mathcal{M}}$ in a given point. Gradient descent is an iterative minimization algorithm for multivariate functions. Let $R \in \mathcal{R}$ be a point in the readout space; we want to find a point $D = (x, y, z) \in \mathcal{D}$ in the detector space such that

$$\bar{\mathcal{M}}(D) = R = (x'_R, y'_R, t_R). \quad (3.9)$$

We define a function f_R in the readout space as a distance in this space:

$$f_R(x', y', t) = \sqrt{(x' - x'_R)^2 + (y' - y'_R)^2 + v_d^2(t - t_R)^2}, \quad (3.10)$$

where v_d is an approximation of the drift velocity in the TPC, obtained from the reconstruction in Section 3.1 (**there will be an image with the linear fit there**). We make an initial guess (**actually in the original code we just take $z = 0$**):

$$D_0 = (x'_R, y'_R, v_d t_R). \quad (3.11)$$

Assuming we have the n -th estimate D_n , we calculate the i -th component of the gradient of $f_R \circ \bar{\mathcal{M}}$ numerically using central differences:

$$\left[\nabla(f_R \circ \bar{\mathcal{M}}) \right]^i(D_n) \approx \frac{f_R(\bar{\mathcal{M}}(D_n + s \cdot e^i)) - f_R(\bar{\mathcal{M}}(D_n - s \cdot e^i))}{2s}, \quad (3.12)$$

where $e^i \in \mathcal{D}$ is the i -th coordinate vector and s is the step size. The step size should be sufficiently small; initially, we set it as a fraction of the map's grid spacing $s = \frac{l}{10}$. During the minimization, we check that $f_R(\bar{\mathcal{M}}(D_n)) < 10s$ at all times. **When using trilinear interpolation, it would be more efficient to calculate the gradient explicitly (\pm same result). This could be implemented inside the *Field* template class.** The next iteration can be calculated as follows:

$$D_{n+1} = D_n - \gamma \nabla(f_R \circ \bar{\mathcal{M}})(D_n), \quad (3.13)$$

where $\gamma \in \mathbb{R}^+$ is the damping coefficient. It should be set to a small enough value to ensure convergence, but large enough for sufficient converging speed.

343 The minimization stops either when the error $f_R(\overline{\mathcal{M}}(D_n))$ drops below a specified
 344 value or when the number of iterations exceeds a certain limit (in this case,
 345 a message is printed into the console). The parameters of this method can be
 346 further optimized (e.g., a better choice of γ , **gradient computation**); instead, we
 347 later decided to use the interpolation on the inverse grid described in the next
 348 section.

349 **Measure reconstruction duration and compare it with the inverse grid inter-**
 350 **polation? Also compare the result? Not sure if this has to be cited.**

351 3.2.2 Interpolation on the Inverse Grid

352 **Interpolating between known points in the readout space. Gaussian elimina-**
 353 **tion, multivariate polynomial. Benefits compared to the gradient descent search**
 354 **method (one-time computation for the whole map is easy to achieve if needed).**

355 The currently used baseline reconstruction method is the interpolation on
 356 the inverse grid. Rather than attempting to invert the trilinearly interpolated
 357 map as in the previous section, we take advantage of the fact that the map $\overline{\mathcal{M}}$
 358 is one-to-one (**isomorphism is supposed to preserve structure, not sure how to**
 359 **interpret that here**). Since we have simulated values of this map on a regular
 360 grid in the detector space \mathcal{D} , we also know the inverse map $\overline{\mathcal{M}}^{-1}$ on the irregular
 361 inverse grid in the readout space \mathcal{R} . To get an approximation of the inverse map
 362 in the entire readout space, we can use interpolation.

363 Since the inverse grid is irregular, trilinear interpolation cannot be applied.
 364 Given that the simulated map is dense enough to provide a good approxima-
 365 tion considering the size of our pads, we can adopt a similar approach (more
 366 complicated and computationally heavy alternative would be natural neighbor
 367 interpolation). As shown in Equation 1.12 in Section 1.1.2, trilinear interpolation
 368 can be expressed as a polynomial:

$$\hat{f}(x, y, z) = axyz + bxy + cxz + dyz + ex + fy + gz + h, \quad (3.14)$$

369 where a, b, c, d, e, f, g, h are coefficients uniquely determined by the values of
 370 the function at the vertices of the interpolation cell. We can generalize this
 371 for a function defined on an irregular grid. Given the function values at any eight
 372 points, we can write a system of eight linear equations

$$\begin{pmatrix} x_1 y_1 z_1 & x_1 y_1 & x_1 z_1 & y_1 z_1 & x_1 & y_1 & z_1 & 1 \\ \vdots & \vdots & \vdots & \vdots & \vdots & \vdots & \vdots & \vdots \\ x_8 y_8 z_8 & x_8 y_8 & x_8 z_8 & y_8 z_8 & x_8 & y_8 & z_8 & 1 \end{pmatrix} \begin{pmatrix} a \\ \vdots \\ h \end{pmatrix} = \begin{pmatrix} f(x_1, y_1, z_1) \\ \vdots \\ f(x_8, y_8, z_8) \end{pmatrix}, \quad (3.15)$$

373 which has a unique solution for the coefficients for most values of (x_n, y_n, z_n) and
 374 $f(x_n, y_n, z_n)$, where $n \in \{1, \dots, 8\}$.

375 This approach introduces a small complication: finding the correct pseudo-
 376 cell (i.e., the image of eight vertices forming a cubic cell in the regular grid) in
 377 the inverse grid. The eight irregularly spaced vertices of this pseudocell do not
 378 define a unique volume, so there are multiple possible ways to partition \mathcal{R} into
 379 pseudocells, with no obvious choice among them.

380 **We are currently ignoring this problem and performing binary search along**
 381 **x, y, z (in this order). It shouldn't matter too much because the 70/30 map**

382 doesn't cause such a big distortion and was even accidentally extrapolated for all
 383 z different from the central plane. Interpolation should be generally faster than
 384 the gradient descent since we don't need to iterate. We also don't need to optimize
 385 it to improve performance, if it's too slow we can even calculate the coefficients
 386 for the entire map before reconstruction.

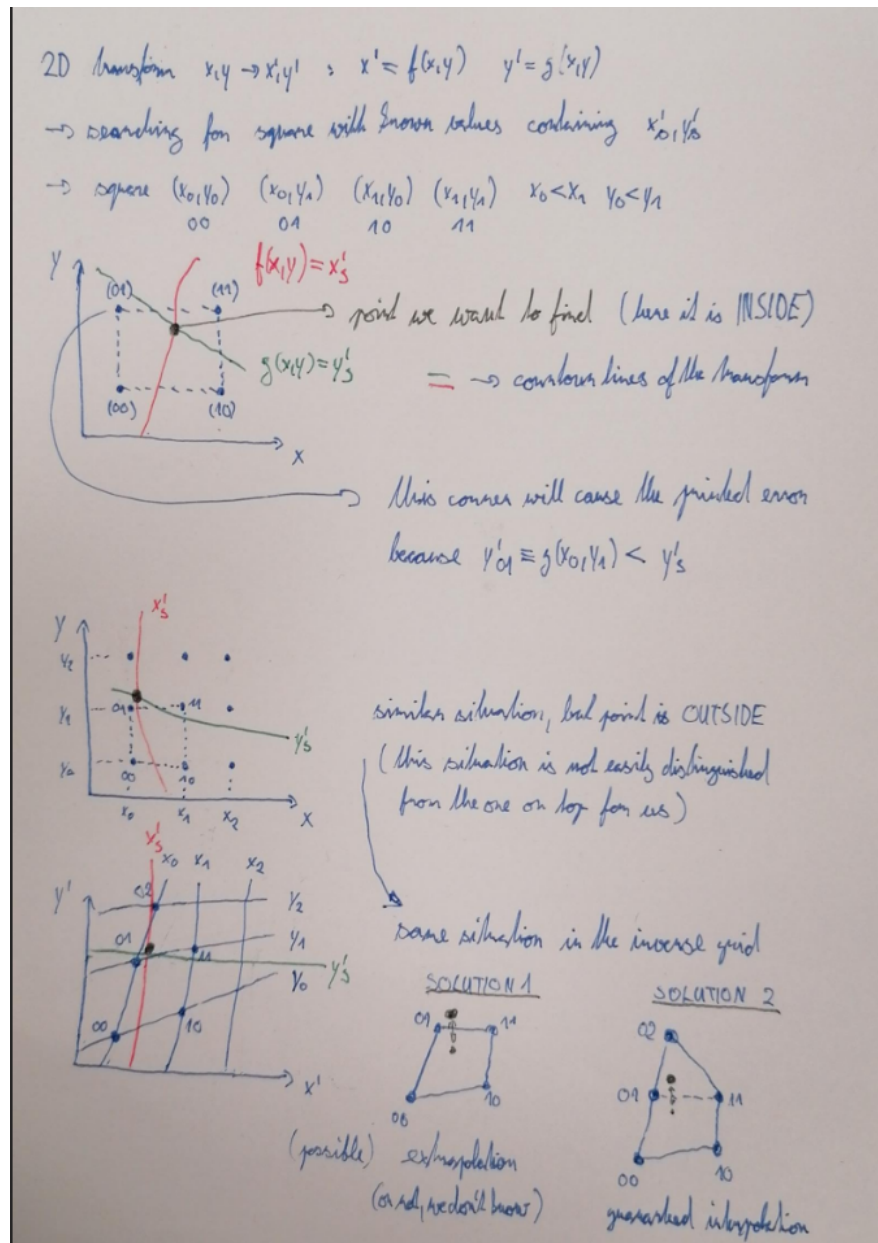


Figure 3.6: Selection of the points for interpolation. Create better images; use the explanation interpolation vs. extrapolation strange property. Solution 2 probably does not make much sense.

387 3.3 Discrete Reconstruction

388 Reconstruction with pads and time bins. Maybe testing different pads. Mapping
 389 the center of the pad (along with the midpoint of the time bin) isn't necessarily

390 the best approach since it might not correspond to the average parameters of
391 an electron with these readout parameters (insignificant?).

392 It is also possible to make this a subsection of the map, making the previous
393 subsections parts of a new subsection 'Map Inversion'.

394 4. Energy Reconstruction

395 The second stage is the reconstruction of the particle's energy using a fit of its
 396 reconstructed track (see Section 3). We have tested three ways of reconstruct-
 397 ing the energy. Fitting is done using the MINUIT algorithm implemented in
 398 ROOT [2]. [Cite some CERN article directly on MINUIT, can add a section.](#)

399 The **Cubic Spline Fit** is a tested and later rejected method of energy re-
 400 construction. It uses smoothly connected piecewise cubic polynomials between
 401 uniformly spaced nodes. Energy is calculated using the fit parameters by comput-
 402 ing the radius of curvature in different points of the fitted curve using the known
 403 magnitude of the magnetic field perpendicular to the trajectory. We rejected this
 404 method because tuning of the fit to have a reasonably stable radius of curvature
 405 turned out to be unpractical.

406 The **Circle and Lines Fit** was chosen as an alternative since this corre-
 407 sponds to the shape of a trajectory of a charged particle crossing a finite volume
 408 with a homogeneous magnetic field. The energy of the particle can be estimated
 409 using the fitted radius and the magnitude of the perpendicular magnetic field in
 410 the middle of the TPC.

411 The **Runge-Kutta Fit** uses the 4th order Runge-Kutta numerical integration
 412 described in Section 2.2. Initial parameters of the track (including the particle's
 413 energy) are optimized so that the integrated trajectory fits to the reconstructed
 414 one. This fit can also be performed as a single parameter (i.e., energy) fit if
 415 we get the initial position and orientation of the particle on the entrance to
 416 the TPC from previous detectors (Timepix 3 (Tpx3) and Multi-Wire Proportional
 417 Chamber (MWPC), see Section 0.2).

418 4.1 Cubic Spline Fit

419 The first attempt to get an early estimate of the kinetic energy of the particle
 420 uses a cubic spline fit. We use an electron track starting in the origin of our
 421 coordinate system with an initial direction in the positive x axis. The example
 422 track is simulated microscopically (see Section 2.1) with a kinetic energy of 8 MeV

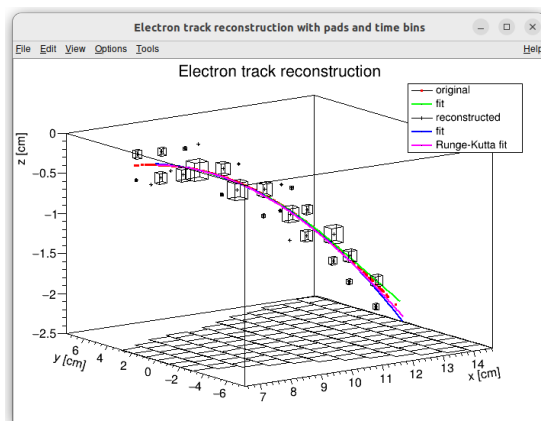


Figure 4.1: Example of a fitted reconstructed track. [Swap for better image.](#)

423 in a gas mixture 90% Ar + 10% CO₂ (the same track was used in Section 3.1).
 424 This track should probably be described in the simulation chapter.

425 In order to calculate the spline, we use the class *TSpline3* from ROOT. This
 426 allows us to evaluate the spline using the coordinates (x_n, z_n) of each node and
 427 the derivatives d_1, d_2 in the first and the last node. We can fit these parameters
 428 of a fixed amount of nodes to the simulated trajectory. We use the IMPROVE
 429 algorithm provided by the *TMinuit* class in ROOT. This algorithm attempts to
 430 find a better local minimum after converging.

431 After the fit, we want to get an energy estimate. In order to calculate it, we
 432 need the radius of curvature, which we get from the fitted spline at every point
 433 of the trajectory. The part of the spline corresponding to a given node is defined
 434 as

$$z(x) = z_n + b\Delta x + c(\Delta x)^2 + d(\Delta x)^3, \quad (4.1)$$

435 where $\Delta x = x - x_n$ and b, c, d are coefficients. Using this equation, we derive
 436 the radius of curvature as:

$$r(x) = \frac{(1 + z'^2(x))^{\frac{3}{2}}}{z''(x)} = \frac{(1 + (b + 2c\Delta x + 3d(\Delta x)^2)^2)^{\frac{3}{2}}}{2c + 6d\Delta x}. \quad (4.2)$$

437 Based on the geometry of the detector, we can assume the magnetic field
 438 $\mathbf{B}(x, 0, z) = (0, B(x, z), 0)$ for a track in the XZ plane. Since the electron is rela-
 439 tivistic, the effect of the electric field on its trajectory is negligible. The Lorentz
 440 force F_L is then always perpendicular to the momentum of the electron and acts
 441 as a centripetal force F_c :

$$\mathbf{F}_L = \mathbf{F}_c, \quad (4.3)$$

$$||e\mathbf{v} \times \mathbf{B}|| = \frac{\gamma m_e v^2}{r}, \quad (4.4)$$

$$ec\beta B = \frac{E_{0e}\beta^2}{r\sqrt{1-\beta^2}}, \quad (4.5)$$

$$\sqrt{1-\beta^2} = \frac{E_{0e}\beta}{ecBr}, \quad (4.6)$$

442

$$\beta^2(x) = \left[1 + \left(\frac{E_{0e}}{ecB(x, z(x))r(x)} \right)^2 \right]^{-1}, \quad (4.7)$$

443 where e is the elementary charge, c is the speed of light in vacuum, m_e is the rest
 444 mass of electron, $E_{0e} = m_e c^2$ is the corresponding energy, γ is the Lorentz factor,
 445 \mathbf{v} is the velocity of the electron, and $\beta = \frac{v}{c}$. We can then finally get our estimate
 446 of the kinetic energy for a given point on the trajectory as follows:

$$E_{\text{kin}}(x) = \left(\frac{1}{\sqrt{1-\beta^2(x)}} - 1 \right) E_{0e}. \quad (4.8)$$

447 We can then average these estimates at multiple points to get one final estimate.
 448 This method was later rejected in favor of the circle and lines fit described in
 449 Section 4.2. Add some figures.

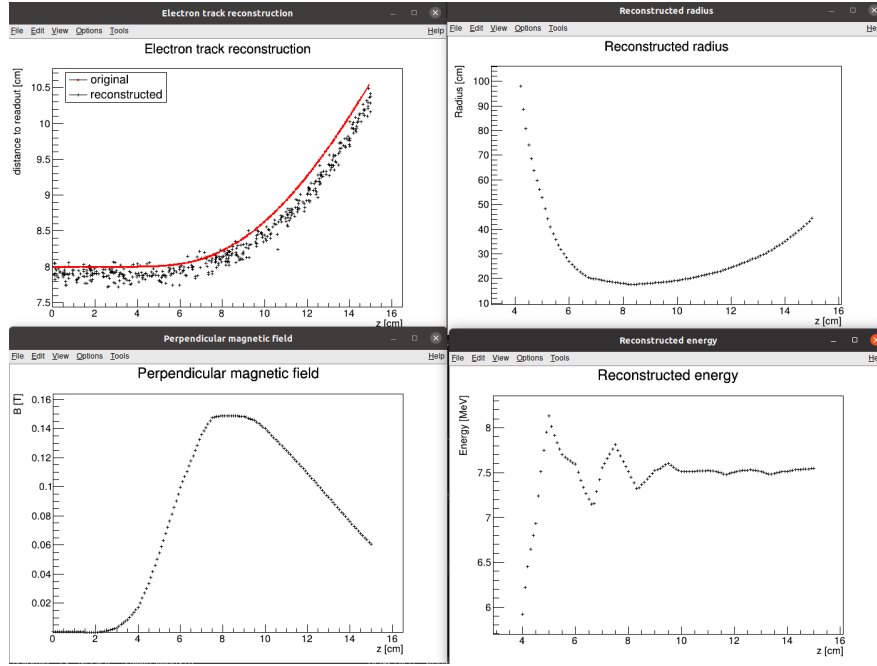


Figure 4.2: First attempt at a track reconstruction using only the drift velocity. Spline energy reconstruction attempt. Swap for better image(s) – subfigure environment, correct coordinates.

4.2 Circle and Lines Fit

Another way to estimate the particle’s kinetic energy is to fit its trajectory with a circular arc with lines attached smoothly. This shape of trajectory corresponds to a movement of a charged particle through a homogeneous magnetic field perpendicular to the particle’s momentum and limited to a certain volume. In general, the shape of such a trajectory in a non-perpendicularly oriented field is a spiral. In our case, this component is negligible since the field is approximately toroidal and the particle motion is nearly perpendicular to it. At first, we tested a 2D version of this fit, then we adapted it to 3D.

Our field is not homogeneous, it is therefore not entirely clear what value of magnetic field should be used along with the fitted radius (using equations 4.7 and 4.8) to get the best estimate for the kinetic energy. Since we only use this method as the first iteration of the particle’s energy that we later refine, an optimal solution of this problem is not required. Instead, we tested two options: taking the value of the field in the middle of the fitted circular arc and taking the average field along it. We haven’t really tried to plot this for multiple tracks, but these estimates are saved somewhere and could be plotted.

4.2.1 Two-dimensional fit

In the 2D case, the fitted function used for the electron track¹ described in Section 4.1 is defined as follows: Maybe describe this track that we used at the beginning somewhere earlier (section microscopic simulations → Testing track?) so that it is easier to refer to it in multiple sections. It is not part of the early GitHub

¹Electron tracks bend towards negative z , we need to use the upper part of the circle

472 commits, so maybe it won't be possible to create exact replicas of the images,
473 but they should be at least very similar.

$$z(x) = \begin{cases} a_1x + b_1 & x < x_1 \\ z_0 + \sqrt{r^2 - (x - x_0)^2} & x_1 \leq x \leq x_2, \\ a_2x + b_2 & x > x_2 \end{cases} \quad (4.9)$$

474 where $a_{1,2}$ and $b_{1,2}$ are the parameters of the lines, (x_0, z_0) is the center of the cir-
475 cle, r is its radius, and $(x_{1,2}, z_{1,2})$ are the coordinates of the function's nodes.
476 That means we have 9 parameters ($z_{1,2}$ are not used in the function) along with
477 2 continuity conditions and 2 smoothness conditions. For the fit, we use the co-
478 ordinates of the nodes and the radius of the circle, which gives us 5 independent
479 parameters (only the radius has to be larger than half of the distance between
480 nodes). The continuity conditions (combined with the relations for $z_{1,2}$) are as
481 follows:

$$z_{1,2} = a_{1,2}x_{1,2} + b_{1,2} = z_0 - \sqrt{r^2 - (x_{1,2} - x_0)^2}. \quad (4.10)$$

482 The smoothness conditions are as follows:

$$a_{1,2} = \frac{x_0 - x_{1,2}}{\sqrt{r^2 - (x_{1,2} - x_0)^2}}. \quad (4.11)$$

483 Equation 4.10 gives us the values of $b_{1,2}$

$$b_{1,2} = z_{1,2} - a_{1,2}x_{1,2}. \quad (4.12)$$

484 For the coordinates of the center of the circle, we can use the fact that the center
485 has to lie on the axis of its chord. In other words, there is a value of a parameter t
486 such that, using the parametric equation of the axis

$$\begin{pmatrix} x_0 \\ z_0 \end{pmatrix} = \begin{pmatrix} \frac{x_1+x_2}{2} \\ \frac{z_1+z_2}{2} \end{pmatrix} + t \begin{pmatrix} \frac{z_2-z_1}{2} \\ \frac{x_1-x_2}{2} \end{pmatrix}. \quad (4.13)$$

487 At the same time, the center has to be in a distance of r from the nodes:

$$(x_1 - x_0)^2 + (z_1 - z_0)^2 = r^2, \quad (4.14)$$

$$\left(\left(\frac{x_2 - x_1}{2} \right)^2 + \left(\frac{z_2 - z_1}{2} \right)^2 \right) t^2 + \left(\frac{x_2 - x_1}{2} \right)^2 + \left(\frac{z_2 - z_1}{2} \right)^2 - r^2 = 0. \quad (4.15)$$

488 Since our electron track bends towards negative z and $x_2 > x_1$, we only care
489 about the solution with $t > 0$

$$t = \sqrt{\frac{r^2}{\left(\frac{x_2 - x_1}{2} \right)^2 + \left(\frac{z_2 - z_1}{2} \right)^2} - 1}, \quad (4.16)$$

490

$$x_0 = \frac{x_1 + x_2}{2} + \frac{z_2 - z_1}{2} \sqrt{\frac{r^2}{\left(\frac{x_2 - x_1}{2} \right)^2 + \left(\frac{z_2 - z_1}{2} \right)^2} - 1}, \quad (4.17)$$

$$z_0 = \frac{z_1 + z_2}{2} - \frac{x_2 - x_1}{2} \sqrt{\frac{r^2}{\left(\frac{x_2 - x_1}{2} \right)^2 + \left(\frac{z_2 - z_1}{2} \right)^2} - 1}. \quad (4.18)$$

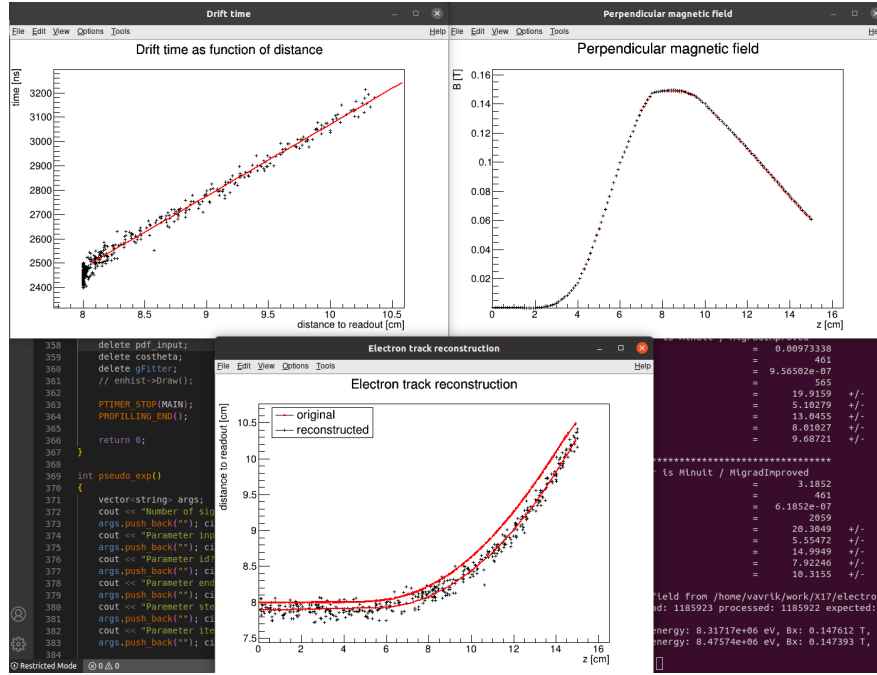


Figure 4.3: First attempt at a track reconstruction using only the drift velocity. Circle and Lines Fit in 2D. Swap for better image, correct coordinates.

491 The function defined in Equation 4.9 along with equations 4.11, 4.12, 4.17 and 4.18
 492 derived using the continuity and smoothness conditions (combined with the re-
 493 lations for $z_{1,2}$) fully define our fitted function with parameters $r, x_{1,2}, z_{1,2}$. Some
 494 pictures of the fit on the tested track. Results of the fit. Again, the actual fit
 495 uses 8-z. Use GeoGebra schematics to generate a picture of 2D geometry.

496 Tested on a Runge-Kutta sample, and with microscopic tracks + map sim-
 497 ulation. Preliminary 2D version (done) and complete 3D version. Geometry of
 498 the fit with its derivation.

499 4.2.2 Three-dimensional fit

500 Explain the geometry and least square method used for the 3D fit.

501 4.3 Runge-Kutta Fit

502 Single parameter fit with 4th order Runge-Kutta simulated track. Future testing
 503 with microscopic simulations and map simulation. Derivation of the geometry
 504 (least squares).

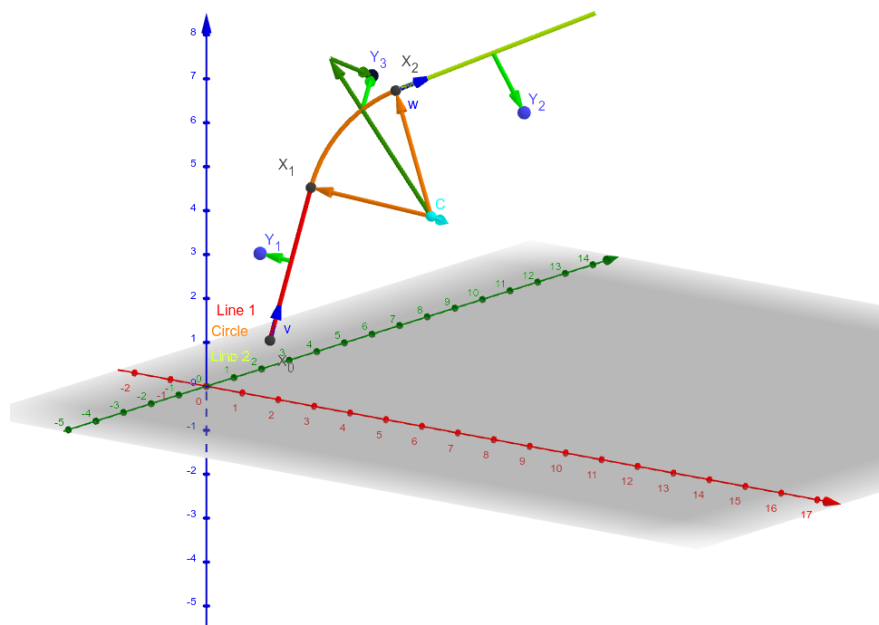


Figure 4.4: Circle and Lines Fit 3D geometry. [Swap for better image.](#)

Conclusion

Here or at the end of each section. Something about the future of this work?

Notes

General notes about the thesis:

- Check that all of the classes and other code are marked the same way in the text. I used italics somewhere, could use different font for this instead.
- Check unbreakable space in front of articles. Remove excessive article usage with proper nouns.
- Currently using margins for single-sided printing (bigger on the left side).
- Check that present tense is used
- American English quotation marks (") instead of British English (').
- Some of the overfull hbox warnings might change if duplex printing is used (they generate black rectangles on the edge of the page), leaving them be for now
- Check nobreakdash usage
- Check capitalized references (e.g., Figure, Section, Equation)

Random notes:

- Only electrons that start and end in the sector closer than 0.5 cm are used for reconstruction (newest version).

Future

Things planned for the future:

- Testing the reconstruction algorithm by measuring real particles with a known energy distribution.
- The **Fast Simulation with Ionization Electron Map** is planned for the future. It will use the HEED program [3] to simulate the primary particle and the Ionization Electron Map (see Section 3.2) to simulate the drift of secondary electrons. It should be significantly faster than the Microscopic Simulation but offer comparable precision since it will rely on an already simulated drift map. (Primary track simulated in HEED. Readout parameters by interpolating the map. Diffusion from the map for randomization.)
- Account for GEM, delta electrons, ...

- Likelihood approach instead of least squares (if it improves the reconstruction significantly), we should at least use a better method than taking the center of the TPC bin.
- More detailed electric field simulation (if needed, GEM will have more complex field)

Likelihood - inverse map

If we wanted to further improve this procedure, taking into account the whole map \mathcal{M} , we could make an "inverse map" from \mathcal{R} to distributions on \mathcal{D} . We could achieve this by taking the normalized probability density of an electron with initial coordinates (x, y, z) having readout coordinates (x', y', t) . If we fix (x', y', t) , we get an unnormalized probability density $f(x, y, z) = \mathcal{M}_{(x, y, z)}(x', y', t)$ (assuming that all initial coordinates are a priori equally likely). This could potentially improve the discrete reconstruction if we take the mean value of this probability density across the pad and time bin

$$f_{\text{pad, bin}}(x, y, z) = \frac{1}{A_{\text{pad}}\Delta t_{\text{bin}}} \int_{\text{pad, bin}} \mathcal{M}_{(x, y, z)}(x', y', t) dx' dy' dt \quad (4.19)$$

and using it for a likelihood fit instead of using least squares. This still assumes that all initial coordinates are equally likely which is clearly not the case for a primary particle track. In the future, we could even use the fast track simulation with the map (should be possible to make around 1000 tracks per minute per core with current settings), create a big set of tracks with reasonable parameters and use these to get an approximation of the probability distribution of the detector response. Some approximations would be necessary when interpreting the data to decrease the degrees of freedom of this distribution (we would have to pick a set of parameters and assume that some of them are independent). This could give us an idea about the best achievable resolution (how significantly will the detector response differ for a given change in energy). If the difference is significant, we could try to further improve the likelihood fit.

Bibliography

- [1] Garfield++. <https://garfieldpp.web.cern.ch/garfieldpp/>. Accessed: 2023-05-18.
- [2] Rene Brun and Fons Rademakers. Root — an object oriented data analysis framework. *Nuclear Instruments and Methods in Physics Research Section A: Accelerators, Spectrometers, Detectors and Associated Equipment*, 389(1-2):81–86, Apr 1997. Proceedings AIHENP’96 Workshop, Lausanne, Sep. 1996, See also <https://root.cern/>, Paper published in the Linux Journal, Issue 51, July 1998.
- [3] I.B. Smirnov. Modeling of ionization produced by fast charged particles in gases. *Nuclear Instruments and Methods in Physics Research Section A: Accelerators, Spectrometers, Detectors and Associated Equipment*, 554(1):474–493, 2005.

List of Figures

575			
576	1.1	Pad layout of the TPC. <i>Swap for better image.</i>	4
577	1.2	Visualization of trilinear interpolation as a composition of linear	
578		interpolations. <i>Image drawn in GeoGebra and inspired by a similar</i>	
579		<i>image on Wikipedia (which looks a bit worse) – is credit necessary?</i>	6
580	2.1	Example of a simulated electron track in 70 % argon and 30 % CO ₂	
581		atmosphere (on the left). <i>Swap for better images, better zoom.</i>	
582		<i>Explain drift lines, primary particle.</i>	8
583	2.2	Comparison of diffusion in a simulated electron track in 70 % ar-	
584		gon, 30 % CO ₂ atmosphere and in 90 % argon, 10 % CO ₂ atmo-	
585		sphere (on the right). <i>Swap for better image, better zoom. Or</i>	
586		<i>put the same pictures for both comparisons in one subfigure, etc.</i>	
587		<i>Describe better.</i>	8
588	3.1	Dependence of the drift time on the z coordinate in 90 % argon	
589		and 10 % CO ₂ atmosphere, fitted with a linear function. The fitted	
590		function gives us the average drift velocity in the gas and can be	
591		used for rough reconstruction in our TPC. <i>Swap for better image</i>	
592		<i>with axis labels, etc. Maybe write the fitted equation.</i>	10
593	3.2	First attempt at a track reconstruction using only the drift velocity.	
594		This approach works well in a standard TPC (<i>ideally cite some</i>	
595		<i>source?</i>). 90 % argon and 10 % CO ₂ atmosphere. <i>Swap for better</i>	
596		<i>image, correct coordinates.</i>	11
597	3.3	First attempt at a track reconstruction using only the drift veloc-	
598		ity, residues. <i>Swap for better image, correct coordinates. What's</i>	
599		<i>causing the shift? Explain details.</i>	11
600	3.4	Example of map generation. <i>Swap for better image, correct coor-</i>	
601		<i>ordinates.</i>	13
602	3.5	Example reconstruction with the map. <i>Swap for better image,</i>	
603		<i>correct coordinates.</i>	14
604	3.6	Selection of the points for interpolation. <i>Create better images; use</i>	
605		<i>the explanation interpolation vs. extrapolation strange property.</i>	
606		<i>Solution 2 probably does not make much sense.</i>	16
607	4.1	Example of a fitted reconstructed track. <i>Swap for better image.</i> .	18
608	4.2	First attempt at a track reconstruction using only the drift velocity.	
609		Spline energy reconstruction attempt. <i>Swap for better image(s) –</i>	
610		<i>subfigure environment, correct coordinates.</i>	20
611	4.3	First attempt at a track reconstruction using only the drift veloc-	
612		ity. Circle and Lines Fit in 2D. <i>Swap for better image, correct</i>	
613		<i>coordinates.</i>	22
614	4.4	Circle and Lines Fit 3D geometry. <i>Swap for better image.</i>	23

⁶¹⁵ List of Tables

616 List of Abbreviations

617 **HEED** High Energy Electro-Dynamics

618 **IEAP CTU** Institute of Experimental and Applied Physics, Czech Technical
619 University in Prague

620 **IPF** Internal Pair Formation

621 **MWPC** Multi-Wire Proportional Chamber

622 **OFTPC** Orthogonal Fields TPC

623 **TPC** Time Projection Chamber

624 **Tpx3** Timepix 3